THE DUST ENSHROUDED QUASAR IN THE ULTRALUMINOUS GALAXY MARKARIAN 463: RADIO, NEAR-INFRARED, AND OPTICAL IMAGING

J. M. MAZZARELLA
Palomar Observatory, California Institute of Technology, Pasadena, California 91125

R. A. GAUME
Center for Advanced Space Sensing, Naval Research Laboratory, Code 4213.6, Washington, DC 20375-5000

B. T. SOIFER, J. R. GRAHAM, G. NEUGEBAUER, AND K. MATTHEWS
Palomar Observatory, California Institute of Technology, Pasadena, California 91125
Received 8 March 1991; revised 3 June 1991

ABSTRACT

New radio continuum, near-infrared, and optical images are presented for the infrared ultraluminous galaxy Mrk 463, which prior optical work has shown to be an interacting/merging system containing two Seyfert 2 nuclei separated by 4″ (4 kpc). The eastern nucleus, Mrk 463E, has a steep-spectrum ($f_\nu \propto \nu^{-1}$) radio core with a luminosity density that is characteristic of a quasar or radio galaxy. Imaging at 20 cm reveals previously unknown components 4″ north and 18″ south of Mrk 463E, and a source 10″ to the northwest which is apparently linked to the nuclear region. The western nucleus, Mrk 463W, has been detected at 6 and 20 cm ($f_\nu \propto \nu^{-0.5}$); it has a radio luminosity comparable to that of a moderately luminous Seyfert galaxy or a highly luminous starburst galaxy. Near-infrared images at wavelengths less than 2.3 μm show the two nuclei; only Mrk 463E has been detected at 3.7 μm. Mrk 463E has an extremely red $V-K$ color of 6.8 mag. Brightness profiles of Mrk 463E are unresolved at K and L' but extended at J; this is likely due to the effects of extinction and centrally concentrated hot dust emission. Radio continuum components 4–18 kpc from the nucleus are aligned with previously known 0.05–1.5 kpc radio structure and extended, conical [O III] emission. This suggests that Mrk 463E is powering weak radio lobes and may therefore exemplify a transition between the confined linear sources in Seyfert galaxies and the extended lobes in classical quasars and radio galaxies. Mrk 463E has a 3.7 μm luminosity and $K-L'$ color comparable to PG quasars, suggesting that dust obscures an embedded quasar. These data are consistent with recent spectropolarimetry observations of Miller & Goodrich [ApJ, 355, 456 (1990)] that reveal a Seyfert 1 nucleus in Mrk 463E. We suggest that Mrk 463 represents the genesis of a classical quasar or radio galaxy.

1. INTRODUCTION

Markarian 463 (= UGC 8850) is an extremely active galaxy at nearly all wavelengths. Early optical studies revealed a peculiar galaxy with two nuclei of nearly the same visual brightness separated by 4″ and surrounded by a diffuse halo and extended plume (Adams 1977; Petrosian *et al.* 1978). Deep CCD imaging shows tidal tails indicative of a merger between two spiral galaxies of nearly equal mass (Mazzarella & Boroson 1987; Hutchings & Neff 1989). Both nuclei exhibit Seyfert 2 spectra (Shuder & Osterbrock 1981; Hutchings & Neff 1989), while optical spectropolarimetry indicates that the eastern nucleus (Mrk 463E) contains an obscured, presumably dust enshrouded, Seyfert 1 nucleus (Miller & Goodrich 1990). *IRAS* observations have shown that Mrk 463 is an ultraluminous ($L_{\rm bol} \gtrsim 10^{12}\ L_\odot$), warm ($f_{25\mu m}/f_{60\mu m} > 0.2$) galaxy that may be in an intermediate stage between dust enshrouded AGNs and classical quasars (Sanders *et al.* 1988b). Mrk 463 is a weak H I source with a narrow velocity profile of 150 km s^{-1} (Hutchings *et al.* 1987). The nuclei have a small redshift difference of $c\Delta z \approx 50$ km s^{-1} (Hutchings & Neff; Mazzarella 1989), consistent with an interacting system in which the bulk of kinematic disturbance lies in the plane of the sky. Recent CO(1→0) observations have shown that Mrk 463 has an H_2 mass of $10^{10}\ \mathcal{M}_\odot$ (Sanders *et al.* 1989).

Mrk 463 is a powerful radio source with a 1.4 GHz luminosity density of 1.5×10^{24} W Hz^{-1}. Radio images have been obtained at 2, 6, and 18 cm with the VLA, MERLIN, and the European VLBI Network (Wilson & Willis 1980; Ulvestad *et al.* 1981; Ulvestad and Wilson 1984; Unger *et al.* 1986; Neff & Ulvestad 1988). These observations reveal small-scale linear structure associated with Mrk 463E which is suggestive of collimated emission along a position angle (P.A.) of $\approx 10°$ over the scale of 0.″05–1.″5 (0.05–1.5 kpc). Hutchings & Neff (1989) present a narrow band [O III] image which shows a conic structure centered on Mrk 463E and a knot located 11″ to the south. The [O III] emission is aligned with the small-scale radio axis, suggesting that Mrk 463E is beaming both radio emitting plasma and ionizing radiation (Hutchings and Neff).

The current work presents new imaging data at radio, near-infrared, and optical wavelengths which provide insight into the processes associated with the ongoing merger and nuclear activity in Mrk 463. The high dynamic range and sensitivity of the radio continuum synthesis images reveal significant new structures, and comparison of the near-infrared and optical imaging data clearly shows the source of the nuclear luminosity. We assume $H_0 = 75$ km s^{-1} Mpc^{-1}, $q_0 = 0.5$, and a distance of 200 Mpc to Mrk 463, so that 1″ corresponds to 1 kpc in projected distance.

 0004-6256/91/041241-12$00.90

2. RADIO CONTINUUM AND OPTICAL IMAGING

Radio synthesis observations of Mrk 463 were obtained using the Very Large Array (VLA) of the National Radio Astronomy Observatory (NRAO).[1] Observations were made at wavelengths of 6 and 2 cm using the C array on 1987 January 22, and again using the C/D array on 1987 February 9. Observations at 20 and 6 cm were made using the A array on 1987 August 14. Primary flux density and polarization calibrations were obtained from observations of 3C 286. Phase calibrators were observed approximately every 20 minutes. After initial editing and calibration of the data, subsequent processing was performed using the AIPS (NRAO). Multiple array observations at a given wavelength were combined in the (u,v) plane to increase sensitivity to weak or extended structures. Effects introduced in the image plane as the result of incomplete sampling of the transform plane were partially corrected by application of an ungridded CLEAN beam deconvolution algorithm (Cornwell & Braun 1989). The signal-to-noise levels in the resulting images were sufficiently high to allow application of an iterative self-calibration technique which refines the complex gains of the individual array elements (Cornwell & Fomalont 1989).

A contour plot of the new 20 cm VLA data is shown in Fig 1(a). The resolution of the image is $2\farcs4\times1\farcs8$ full width at half maximum (FWHM) at P.A. $= -56°$. The image was made with natural (equal) weighting of the data points in the transform plane which results in the greatest sensitivity to weak emission. In order to compare the spatial scales of known radio structures in Mrk 463, Fig. 1(b) shows 18 cm MERLIN data from Unger *et al.* (1986) and Fig. 1(c) shows 18 cm European VLBI Network data from Neff & Ulvestad (1988). Figure 2 is a contour plot of the 20 cm emission at a resolution of $1\farcs6\times1\farcs3$ made by applying a uniform weighting to the data in the transform plane, where each data point is weighted by the local data density. Uniformly weighted data generally results in images with improved resolution, but at the cost of sensitivity to weak structure. Mrk 463E is also a weak source of linearly polarized 20 cm emission, with 0.5% polarization at P.A. $\approx -45°$. Since polarization measurements at other radio frequencies are unavailable, it is not possible to correct for possible Faraday rotation to derive the intrinsic projected magnetic field direction.

Figure 3(a) is a 6 cm image made with uniform weighting of the (u,v) data, resulting in a resolution of $0\farcs3\times0\farcs4$ (P.A. $= -64°$). Figure 3(b) is an image made from the same data with a Gaussian weighted taper applied to the data as a function of radius from the origin of the (u,v) plane. The 30% weighting level of the Gaussian taper was at a radius of 150 $k\lambda$, resulting in a resolution of $1\farcs2\times1\farcs0$ (P.A. $= -66°$). The component 1".3 south of Mrk 463E was detected prior to these observations at 6 cm (Ulvestad *et al.* 1981) and at 2 and 18 cm (Unger *et al.* 1986; Neff & Ulvestad 1988). A 2 cm uniform weighted image of Mrk 463 with a resolution of $2\farcs1\times1\farcs2$ (P.A. $= -80°$) is shown in Fig. 4. Only Mrk 463E is detected, but the 2 cm contours suggest the presence of the source 1".3 south of Mrk 463E.

The high dynamic range and sensitivity of the new VLA images reveal a number of features not detected in previous observations. First, the western nucleus (Mrk 463W) has been detected at 20 and 6 cm. Mrk 463W is located 4" away, almost due west from Mrk 463E. The 20 cm luminosity of Mrk 463W is only 1.0% that of Mrk 463E. Second, Fig. 1(a) shows components 4" north (see also Fig. 2) and 18" south of Mrk 463E, in addition to a weak filament extending 10" northwest of Mrk 463W. The rms background noise in the image is 0.17 mJy beam^{-1}. There are a few noise peaks at 0.77 mJy beam^{-1} (4.5σ), but the peak signal in the northwest feature is 1.05 mJy beam^{-1} (5.6σ) and there are a number of pixels in this feature at $>5\sigma$. However, much of the emission that connects the northwest source to the nuclear region is only at the 3.5σ level. Therefore, while the peak in the northwest structure is a confident detection, the faint emission linking it to the nuclei is less certain and merits confirmation. Table 1 lists flux densities and luminosities for measured features, as well as spectral indices for the nuclei.

Optical images in the B and V bands were obtained using an RCA CCD on the 1.3 m McGraw-Hill Telescope of the Michigan–Dartmouth–MIT Observatory on 6 April and 31 December 1986. The data were reduced, calibrated, and coadded as described by Mazzarella (1989). Figure 5 displays 20 cm contours superposed on a gray-scale representation of a B band image of Mrk 463. Because the separation and position angle between the nuclei are the same in the optical and radio synthesis images, it was assumed that the optical and radio nuclei coincide.

The B image agrees with that of Hutchings & Neff (1989). Although no image was taken in the [O III] line, the redshifted [O III] emission lines are in the V filter, and the [O III] emission discovered by Hutchings & Neff is seen in the $B-V$ color map presented in Fig. 6. The 20 cm feature 18" to the south of Mrk 463E lies along the axis defined by the [O III] emission, just south of the bright [O III] knot. The 20 cm component 4" to the north is also roughly aligned with this axis (cf. Figs. 2 and 6).

3. NEAR-INFRARED ARRAY IMAGING

Near-infrared images at J (1.25 μm), H (1.65 μm), K (2.20 μm), and L' (3.7 μm) were obtained using the Cassegrain Infrared Camera on the 5 m Hale Telescope of Palomar Observatory on 1990 May 9 UT. The image scale was 0".31 per pixel and the field of view was $18''\times19''$. The seeing was 0".75 FWHM at 2.2 μm. The observations consisted of obtaining images of Mrk 463 and regions of adjacent blank sky. Successive observations were offset a few arcseconds to allow removal of bad pixels and to shift potential background sources in the reference sky images. After linearization of the raw data, a median sky image was constructed from five or more sky frames in each filter. The median sky frame was then offset to the background level of each individual sky frame before subtraction from the source frame nearest in time. This method insures subtraction of the correct sky level appropriate for each frame, while improving the sky signal-to-noise ratio and removing background sources which may otherwise contaminate individual sky frames. The images were flattened with normalized twilight sky images (after dark subtraction), aligned using the centroids of the nuclei, and coadded. The L' images were flattened using a median of the dithered dark sky observations. Photometric calibration was performed using observations of standard stars from the list of Elias *et al.* (1982). Figure 7 presents J and K images of the nuclear region of Mrk 463. Both nuclei appear as point sources in an extended envelope

[1] The National Radio Astronomy Observatory is operated by Associated Universities, Inc., under cooperative agreement with the National Science Foundation.

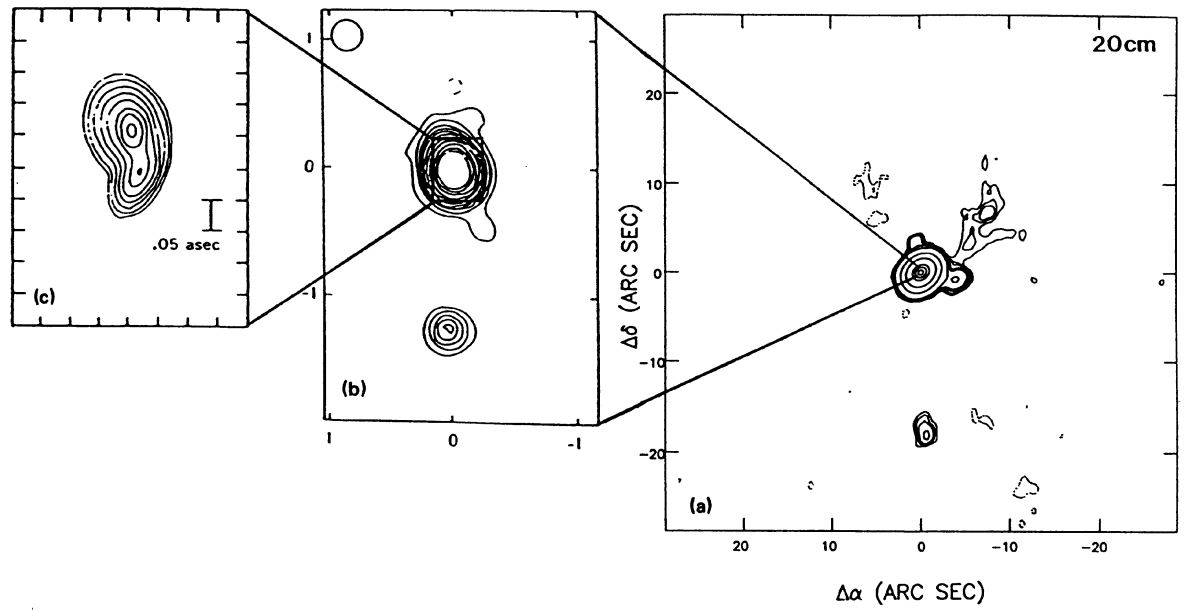

FIG. 1. (a) New 20 cm VLA data contoured from 3 times the rms background noise of 0.18 mJy beam^{-1}. The dashed contours in this and following contour plots indicate the -3σ level. Contours are drawn at -0.2%, 0.2%, 0.26%, 0.3%, 0.4%, 0.5%, 0.9%, 5%, 20%, 60%, 80%, and 95% of the peak flux density of 299.1 mJy beam^{-1}. The image was made with natural weighting of the (u,v) data in the transform plane resulting in a resolution of $2''.4 \times 1''.8$ (FWHM) at P.A. $= -56°$. North is up and east is to the left in all images. The origin of the arcsecond offsets in this and following figures is the centroid of Mrk 463E at $\alpha = 13^h\,53^m\,39^s.79$, $\delta = +18°36'57''.6$ (1950). Mrk 463W is located 4″ just south of west from Mrk 463E. (b) 18 cm (1.66 GHz) MERLIN data from Unger *et al.* (1986). (c) 18 cm European VLBI Network data from Neff & Ulvestad (1988).

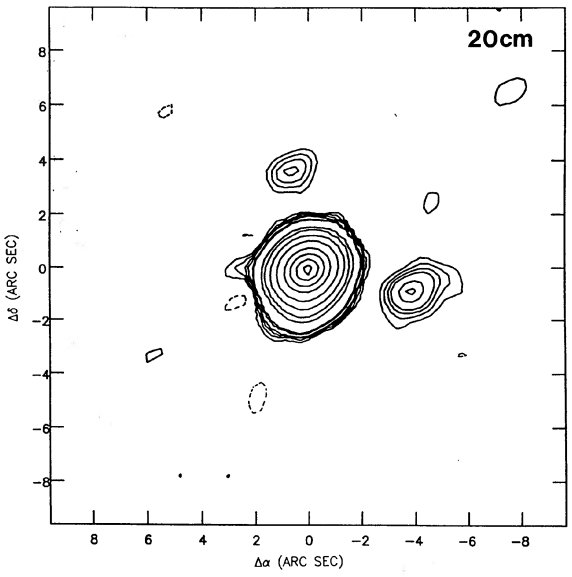

FIG. 2. 20 cm data mapped with uniform weighting for maximum resolution. Contours are drawn from 3 times the rms background of 0.17 mJy beam^{-1}, or -0.2%, 0.2%, 0.3%, 0.4%, 0.5%, 0.75%, 0.9%, 3%, 5%, 10%, 20%, 40%, 60%, 80%, and 95% of the peak flux density of 283.7 mJy beam^{-1}. The resolution of the image is $1''.6 \times 1''.3$ at P.A. $= -63°$.

at *J*, *H*, and *K*. The *L'* image shows only a point source centered on Mrk 463E. Morphological details in the underlying galaxies are best visible at *J*. The dominant feature in the *J* band image, in addition to the two nuclei, is a flattened barlike morphology.

Table 2 presents the results of photometry performed in synthesized beams centered on the two nuclei, and for the integral measurements, between the nuclei. No attempt has been made to remove the galaxy background from the nuclear measurements; the quoted magnitudes and uncertainties are the result of simple numerical aperture photometry. Scatter in the photometric zero points for the night dominate the uncertainties in the near-infrared magnitudes. The array measurements agree with single-channel photometry using a 10″ diameter beam (Sanders *et al.* 1988b) to within 3%. Brightness profiles along a line through the nuclei at P.A. = 79° are plotted in Fig. 8. In this figure, the near-infrared data have been smoothed to match the 1″.5 resolution of the optical brightness profiles which are plotted for comparison. The data show that Mrk 463W is slightly brighter than Mrk 463E in the *B* band. The near-infrared data reveal an increasing dominance of Mrk 463E over Mrk 463W with increasing wavelength; at *L'* Mrk 463E is $\gtrsim 5$ mag brighter than Mrk 463W. The internal reddening for the nuclei of Mrk 463 has been estimated from the observed Hα/Hβ ratio by Shuder & Osterbrock (1981) and Mazzarella & Boroson (1991). Both groups find that the inferred extinction for Mrk 463W is larger than for Mrk 463E, with mean

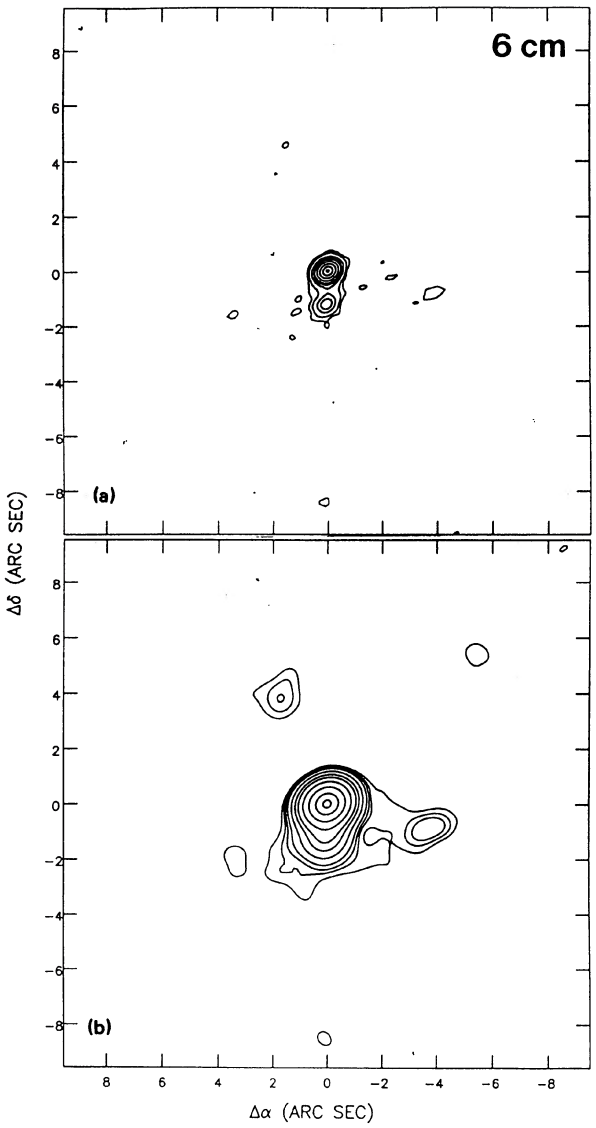

FIG. 3. (a) 6 cm image made with uniform weighting to reveal close secondary component 1".3 south of Mrk 463E; the contour levels are −0.5%, 0.5%, 1%, 3%, 6%, 10%, 20%, 40%, 70%, and 95% of the peak flux density of 74.4 mJy beam^{-1}. (b) Same 6 cm (u,v) data tapered to emphasize emission associated with Mrk 463W; the contour levels are −0.5%, 0.5%, 0.75%, 1%, 1.5%, 3%, 6%, 10%, 20%, 40%, 70%, and 95% of the peak flux density of 84.6 mJy beam^{-1}. The resolution is 0".3×0".4 (P.A. = −64°) and 1".2×1".0 (P.A. = −66°) for images (a) and (b), respectively. The rms background in both images is 0.11 mJy beam^{-1}.

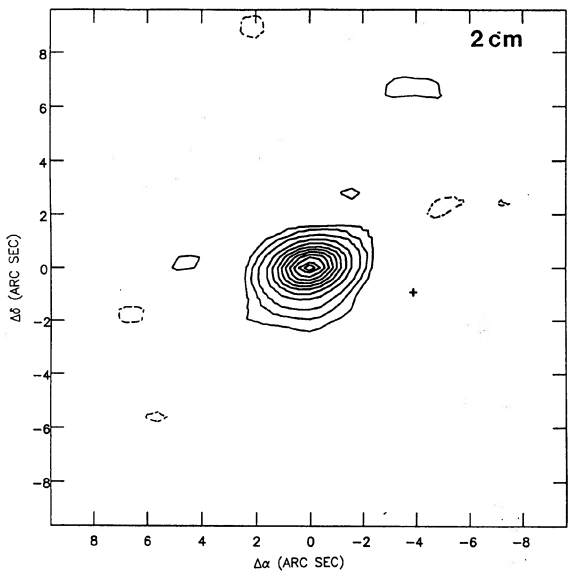

FIG. 4. 2 cm map contoured from 3 times the rms background of 0.19 mJy beam^{-1}. Only Mrk 463E is detected. The position of Mrk 463W is indicated with a plus sign. The resolution is 2".1×1".2 at P.A. = −80°. The contour levels are −2%, 2%, 5%, 10%, 20%, 30%, 40%, 50%, 60%, 70%, 80%, and 90% of the peak flux density of 26.6 mJy beam^{-1}.

E($B-V$) values of 0.7 and 0.4 mag, respectively. However, near-infrared data suggest that extinction affects Mrk 463E more drastically than Mrk 463W (cf., Table 2), and do not suggest that the intrinsic nuclear colors are similar. The Galactic reddening in the direction of Mrk 463 is essentially zero (Burstein & Heiles 1984). Further discussion of reddening and the intrinsic luminosities of the nuclei is given in Secs. *4.2* and *4.3*.

4. DISCUSSION

4.1 Radio Properties

A principal result of the current work is the detection of 20 cm components located 4" (4 kpc) north and 18" (18 kpc) south of Mrk 463E [cf., Figs. 1(a) and 2]. Figure 5 shows that the southern 20 cm component lies near the periphery of Mrk 463. We deduce that this source is associated with Mrk 463E because: (a) there is only a 1% chance of observing a 20 cm source in the flux density range 0.6–1.0 mJy in a random solid angle of sky 30" in radius (Condon 1984); (b) it is projected along the same axis as the small-scale radio emission 0".05–1".5 from Mrk 463E along P.A. ≈ 10° [cf., Figs. 1 and 3(a)]; (c) it is located along the same axis as the linear [O III] emission and knot detected by Hutchings & Neff (1989) (cf., Fig. 6); (d) the contours of the southern component indicate it is edge brightened on the side facing away from the nucleus, much like a classical radio lobe [cf., Fig. 1(a)]; (e) the 20 cm source located 4" slightly east of north from Mrk 463E (cf., Fig. 2) is located roughly along the same axis on the other side of the nucleus, in accord with the hypothesis of collimated ejection from the nucleus in both directions; and (f) the core to lobe distance in Mrk 463 is consistent with the linear size versus radio luminosity relation for Seyferts and radio galaxies (Ulvestad & Wilson 1984).

The data therefore suggest that the central energy source in Mrk 463E powers a radio source 18 kpc to the south, near the faintest optical isophotes of the merging disks. This component will hereafter be referred to as a "lobe." Similarly, the morphology of the 20 cm emission to the northwest of the nuclei suggests one of the nuclei has ejected radio-emitting plasma as far as ≈12 kpc to the northwest. Neither the

TABLE 1. Radio properties.

Feature	Coordinates		f_ν(mJy)			L_ν (W Hz^{-1})[a]			Spectral Index
	α(1950)	δ(1950)	20 cm	6 cm	2 cm	20 cm	6 cm	2 cm	α^b
(1)	(2)	(3)	(4)	(5)	(6)	(7)	(8)	(9)	(10)
Mrk 463E	13 53 39.85	+18 36 57.3	322.5 ± 11.2	100.2 ± 3.5	30.5 ± 0.3	1.5×10^{24}	4.8×10^{23}	1.5×10^{23}	-0.97 ±0.04
Mrk 463W	13 53 39.57	+18 36 56.5	3.2 ± 0.2	1.8 ± 0.3	<0.8	1.5×10^{22}	8.7×10^{21}	$< 3.8 \times 10^{21}$	-0.48 ±0.14
Northern Source	13 53 39.88	+18 37 01.0	1.6 ± 0.1	1.1 ± 0.4	<0.8	7.7×10^{21}	5.3×10^{21}	...	...
Southern Source	13 53 39.80	+18 36 39.1	1.1 ± 0.2	<0.6	<0.8	5.3×10^{21}	...	...	...

Notes to TABLE 1

[a]Luminosity density calculated assuming a distance of 200 Mpc.

[b]$f_\nu \propto \nu^\alpha$. See text for discussion of spectral index calculations and error estimates.

Note: Mrk 463E is detected in linearly polarized 20 cm emission. The emission is only 0.52% (±.04%) polarized at a position angle of ≈ −45°.

northwest peak nor the emission apparently connecting it to the nuclear region correspond to any obvious structure in the near-infrared or optical images.

Very extended radio structures are rare among Seyfert galaxies; linear double and triple radio structures in Seyferts are generally found within a few kpc from the nucleus. Ulvestad & Wilson (1984; 1989) have mapped a large sample of nearby Seyfert galaxies at 20 cm with the VLA, and among those with linear structures, the total sizes range between 0.3 kpc (NGC 2733) and 5.8 kpc (NGC 4388). The mean linear extent of the structures in their sample is 1.7 kpc, corresponding to a typical core-to-lobe distance of ≈0.9 kpc. This is an order of magnitude smaller than the distant components seen in Mrk 463.

In their survey of nearby Seyfert galaxies, Ulvestad and Wilson focused primarily on nuclear and near-nuclear properties; maps for these sources were generally not examined for widely extended features (Ulvestad 1990). In addition, their maps have lower dynamic range than the current data for Mrk 463. Thus relatively weak, large-scale lobes cannot be ruled out in other Seyfert galaxies. However, Mrk 463E has a 20 cm luminosity density which is ≈700 times greater than the mean luminosity density of nearby Seyferts, and the sample of Ulvestad and Wilson is on average eight times closer than Mrk 463. Furthermore, radio observations of Seyfert galaxies which are sensitive to large structures have not revealed emission extended beyond ≈5 kpc (de Bryun & Wilson 1976, 1978). One exception is Mrk 231, which has 20 cm emission reaching ~25 kpc south of the nucleus (Hutchings & Neff 1987); however, the diffuse, extended nature of this emission suggests that it may not be associated with a jet. Ulvestad & Wilson (1984) pointed out that Seyfert galaxies have less powerful radio sources and correspondingly smaller projected linear sizes than radio galaxies. The large projected linear extent of 18 kpc (core to lobe) and the strong 20 cm luminosity density of 1.5×10^{24} W Hz^{-1} place Mrk 463 midway between the Seyferts and radio galax-

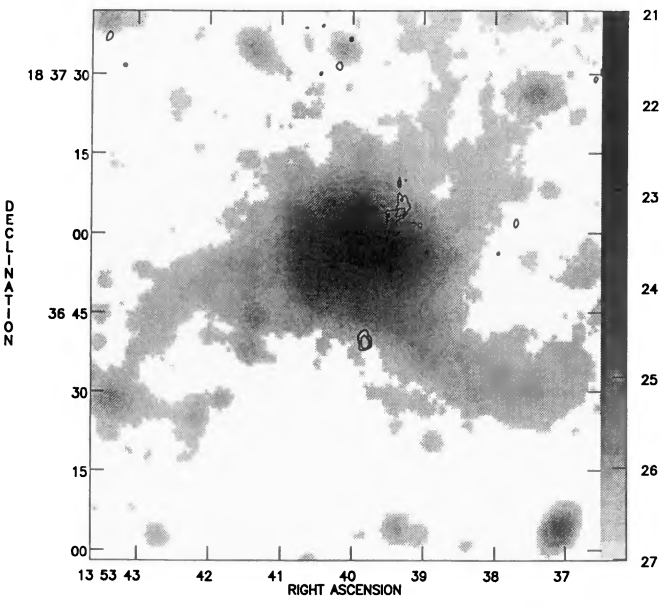

FIG. 5. The 20 cm image (natural weighting) overlaid on a calibrated optical B band image. The gray levels range from 21 to 27 B mag arcsec^{-2}, as indicated in the side bar. The plot axes are equinox 1950.0 coordinates.

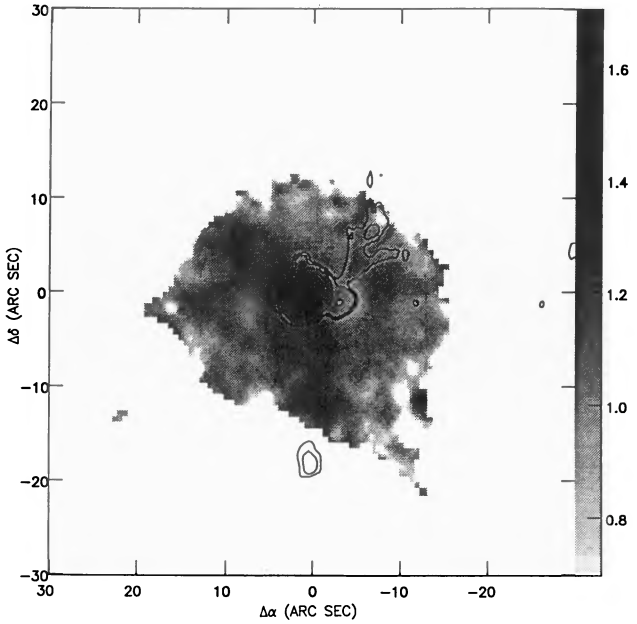

FIG. 6. The 20 cm image (natural weighting) overlaid on an optical $B - V$ color map. The gray scales run from 0.7 to 1.7 mag in $B - V$, as indicated on the side bar. Dark (red) regions associated with the conic [O III] emission discovered by Hutchings & Neff (1988) can be seen joining Mrk 463E and the [O III] knot 11″ to the south. A 20 cm continuum component is located 4″ south of the [O III] knot.

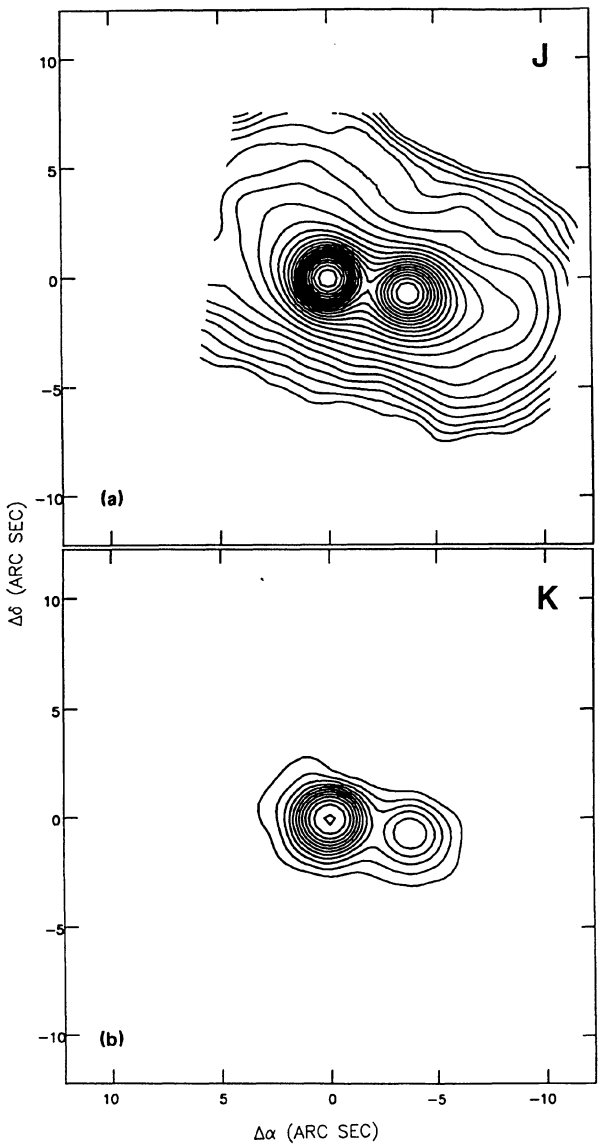

FIG. 7. (a) J (1.25 μm) image contoured from 15 to 20 J mag arcsec^{-2} in steps of 0.2 J mag arcsec^{-2}; (b) K (2.20 μm) image contoured from 11.5 to 17 K mag arcsec^{-2} in steps of 0.5 K mag arcsec^{-2}. The incomplete contour edges in the J image are an artifact of the small field of view and rotation of the image in software for registration with the optical and radio images. The L' (3.7 μm) image is not shown because it simply reveals a point source associated with Mrk 463E.

ies examined by Ulvestad and Wilson. The projected linear size of Mrk 463 is also similar to the smallest 3CR quasistellar radio sources examined by Barthel (1989), which includes a few compact steep-spectrum sources. These considerations support the hypothesis that Mrk 463 represents a transition case between the confined radio sources in Seyfert nuclei and the widely extended radio structures in classical quasars and radio galaxies.

Radio structures with large core-lobe distances are common among radio galaxies which are generally peculiar ellipticals, but rare in confirmed disk galaxies. Double radio lobes extending 15 kpc from the nucleus of the infrared luminous galaxy *IRAS* 04210 + 0400 have been interpreted by Beichman *et al.* (1985) as a transition case between Seyfert (spiral) galaxies and classical radio (elliptical) galaxies. However, Hill *et al.* (1988) suggest that *IRAS* 04210 + 0400 is not a spiral galaxy, but a classical FR I radio galaxy which is unusually dusty and contains a strong nuclear source of ionizing radiation. Mrk 463E has a 20 cm radio luminosity density 10 times greater than *IRAS* 04210 + 0400. Furthermore, numerical simulations of colliding galaxies indicate that the formation of two long tidal tails such as those observed in Mrk 463 require an encounter between two disk galaxies of similar mass (e.g., Toomre & Toomre 1972; Barnes and Hernquist 1991). Mrk 463 therefore represents a rare, if not unique, situation in which a strong radio source with a relatively large core-lobe distance is observed in a disk host galaxy.

4.2 Spectral Energy Distribution and Near-Infrared Properties

Figure 9 displays the spectral energy distributions of the components of Mrk 463 using available data for the nuclei and the integral system. It is notable that Mrk 463E dominates the spectral energy distribution of the integral system at $\lambda \geqslant 3.7$ μm. The near-infrared flux density increases with wavelength in Mrk 463E, and decreases with wavelength in Mrk 463W. This suggests that the mid- to far-infrared emission which dominates the total energy output is highly concentrated in the eastern nucleus. However, a significant contribution by Mrk 463W to the *IRAS* measurements for the integral system cannot be ruled out. Table 2 shows that the near-infrared emission is dominated by the two galactic nuclei. The K image in Fig. 7 makes unlikely the suggestion of Neff & Ulvestad (1988) that the radio component located 1.″3 south of Mrk 463E [cf., Fig. 3(a)] might be associated with a (third) nucleus in this system. This further suggests that this radio component is part of a jet structure aligned out to 18″ from the nucleus (cf., Fig. 1).

For comparison with the photometry in Table 2 (2″ diameter beam), the Palomar–Green (PG) quasars observed by Neugebauer *et al.* (1987) have median rest-frame luminosities, $L = \nu L_\nu$, of $L_V = 6.1 \times 10^{11}\ L_\odot$, $L_K = 1.3 \times 10^{11}\ L_\odot$, and $L_{L'} = 1.4 \times 10^{11}\ L_\odot$. The observed visual luminosity of Mrk 463E, $L_V = 3.1 \times 10^9\ L_\odot$, is not close to even the faintest quasars. However its L' luminosity of $1.2 \times 10^{11}\ L_\odot$ is comparable to the median L' luminosity of PG quasars. In addition, the $K - L'$ color of Mrk 463E, 2.1 mag, is similar to the mean $K - L'$ color of measured PG quasars, 1.7 ± 0.2 mag. If Mrk 463E has an intrinsic $V - K$ color within the range of measured PG quasars (1.5–4.0 mag), its extremely red color of $V - K = 6.8$ mag suggests the optical continuum emission from the obscured Seyfert 1/quasar is originating behind a dust shroud with $A_V \approx 3$–6 mag. This is ≈ 1.5–4.5 more magnitudes of visual extinction that is indicated by the Hα/Hβ line ratio, $A_V \approx 1.2$ mag (Shuder & Osterbrock 1981; Mazzarella & Boroson 1991). We therefore suggest that Mrk 463E would appear as an optical quasar save for the obscuration.

Figure 10 shows the result of normalizing the brightness profiles for each nucleus separately for comparison with the point spread function (PSF) obtained by observing a star at K (0.″8 FWHM) with the same integration time and guiding conditions as the galaxy observations. The PSF was not mea-

TABLE 2. Near-infrared and optical photometry.

Feature	Beam (arc sec)	Apparent Brightness (mag)						log νL_ν ($L_\odot$)			
		B	V	J	H	K	L′	B	V	K	L′
(1)	(2)	(3)	(4)	(5)	(6)	(7)	(8)	(9)	(10)	(11)	(12)
Mrk 463E	2	18.61 ± .05	17.25 ± .05	13.96 ± .07	12.22 ± .07	10.43 ± .06	8.35 ± .12	9.16	9.50	10.88	11.08
	4	17.51 ± .04	16.20 ± .04	13.60 ± .07	12.06 ± .07	10.32 ± .06	8.22 ± .11	9.60	9.92	10.92	11.13
Mrk 463W	2	18.58 ± .05	17.75 ± .05	14.67 ± .07	14.02 ± .07	13.50 ± .07	...	9.17	9.30	9.69	...
	4	17.38 ± .04	16.62 ± .04	14.07 ± .07	13.45 ± .07	12.90 ± .07	...	9.65	9.75	9.89	...
Combined	10	16.11 ± .03	15.12 ± .03	12.81 ± .07	11.71 ± .08	10.16 ± .06	8.3 ± .1	10.16	10.35	10.99	11.14
	15	15.72 ± .03	14.77 ± .03	12.59 ± .07	11.48 ± .08	10.11 ± .06	8.3 ± .1	10.31	10.49	11.01	11.14
	40	15.14 ± .06	14.28 ± .03	...	...	...	...	10.55	10.68	...	...

Notes to TABLE 2

Column (1): Measured feature.
Column (2): Synthesized beam diameter used for numerical aperture photometry (arcsec); 1″ projects to 1 kpc assuming a distance of 200 Mpc. The optical CCD data allow measurements of the combined system out to a beam diameter of 40″.
Columns (3) – (8): Apparent brightness (mag), uncorrected for reddening. No attempt has been made to remove the galaxy background from the nuclear measurements. Scatter in the photometric zero-points for the night dominate the uncertainties in the near-infrared magnitudes.
Columns (9) – (12): Rest-frame luminosity, $\nu L_\nu = 4\pi d^2 \nu f_\nu$ in solar units ($L_\odot = 3.826 \times 10^{26}$ W), where d is the luminosity distance assuming H_o =75 km s^{-1} Mpc^{-1} and $q_o = 0.5$. These values are not corrected for reddening for reasons discussed in the text.

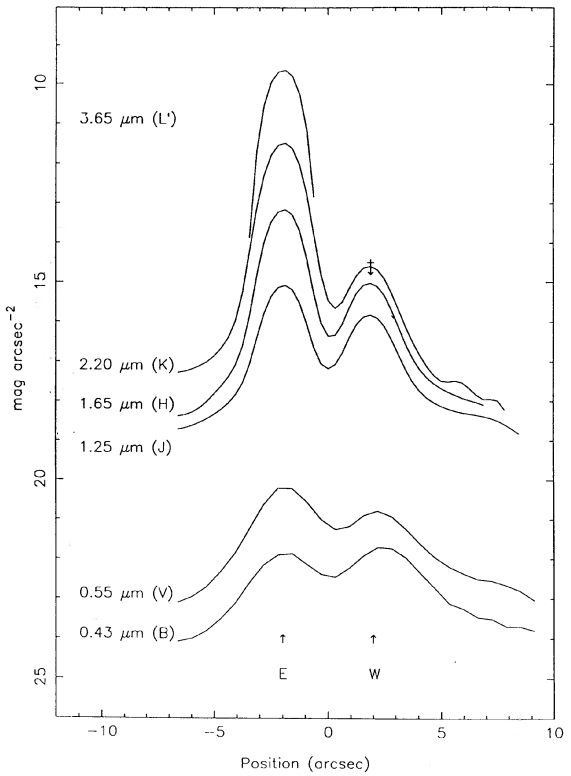

FIG. 8. Calibrated brightness profiles through the nuclei at P.A. = 79°. The near-infrared data have been smoothed to match the resolution of the optical brightness profiles which are plotted for comparison. The relative positions of the two nuclei are labeled; the origin of the arcsecond offsets is arbitrarily chosen between the two peaks. The upper limit to the surface brightness of Mrk 463W at L' is indicated.

sured contemporaneously at J and L'. However, the camera focus is achromatic, and its intrinsic PSF is much smaller than the seeing. If the observed PSF is dominated by atmospheric seeing parametrized via FWHM $\propto \lambda^{-0.2}$, based on the K measurement one expects 0″.9 and 0″.7 FWHM at J and L', respectively. The spatial profiles plotted in Fig. 10 were computed by making cuts along the north–south direction. While Mrk 463E is marginally resolved at J(1″.0), it is unresolved at K and L'. In contrast, Mrk 463W is clearly resolved at K (1″.2 FWHM).

The simplest interpretation of the near-infrared photometric data and brightness profiles is that Mrk 463E harbors a compact source of hot dust emission heated by an intense UV radiation field emanating from a quasar core. This hot dust emission is seen predominantly at K and L'. Dust emission at L' ($T_d \sim 800$ K) is characteristic of a radius of ~ 1 pc from the central UV source (Phinney 1989). The hot dust emission may originate from a geometrically and optically thick torus surrounding the broad line region and quasar core. These observations may therefore directly reveal the dust torus which obscures the Seyfert 1 nucleus observed by Miller & Goodrich (1988).

4.3 The Nature of the Nuclei

All available data point to Mrk 463E being an active nucleus. The evidence presented here includes a compact source of hot dust emission with an L' luminosity comparable to PG quasars, and 20 cm radio components which are ~ 10 times more distant from the nucleus than those observed in typical Seyfert galaxies. The observation of a broad (FWHM = 3000 km s^{-1}) Hβ emission line in the optically polarized flux of Mrk 463E is the most direct observation of a dust enshrouded Seyfert 1 nucleus (Miller & Goodrich 1990).

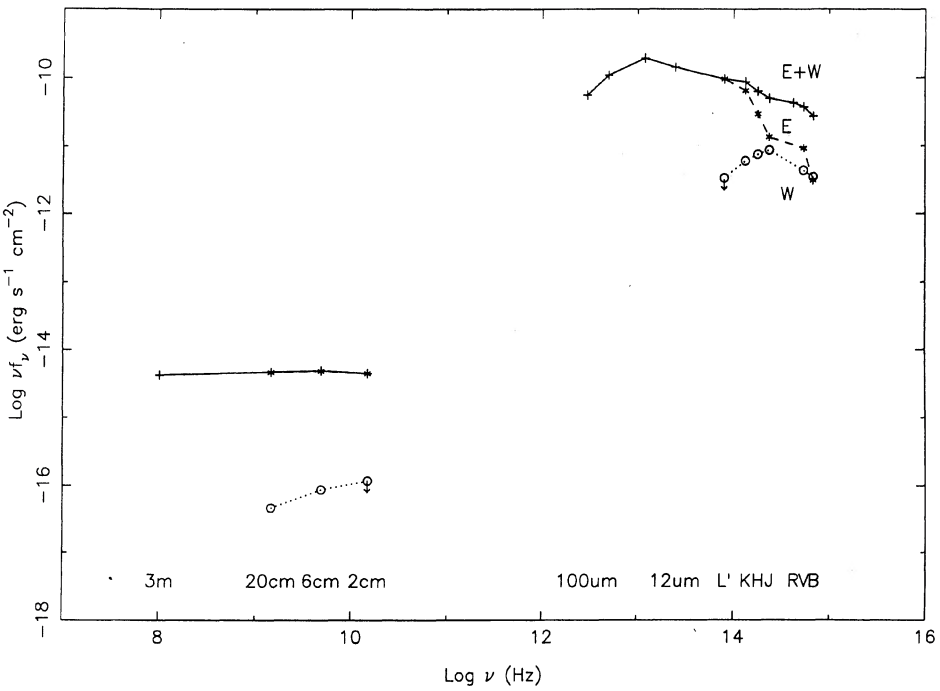

FIG. 9. Spectral energy distribution for the integral system (solid line and plus signs), Mrk 463E (dashed line and asterisks), and Mrk 463W (dotted line and circles). The arrows indicate upper limits at 3.7 μm and 2 cm for Mrk 463W. The optical and near-infrared magnitudes were converted to f_ν units using the calibrations in Neugebauer *et al.* (1987). The *U* band measurement for the integral system is from Peterson *et al.* (1981). The *BVJHKL'*, 2, 6, and 20 cm data are from this work; far-infrared measurements are the *IRAS Point Source Catalog* data for the integral system; 2.9, 3.7, and 11 cm data for the integral system are from Kojoian *et al.* (1976); the 3 m measurement is from Artyukh & Vetukhnovskaya (1983).

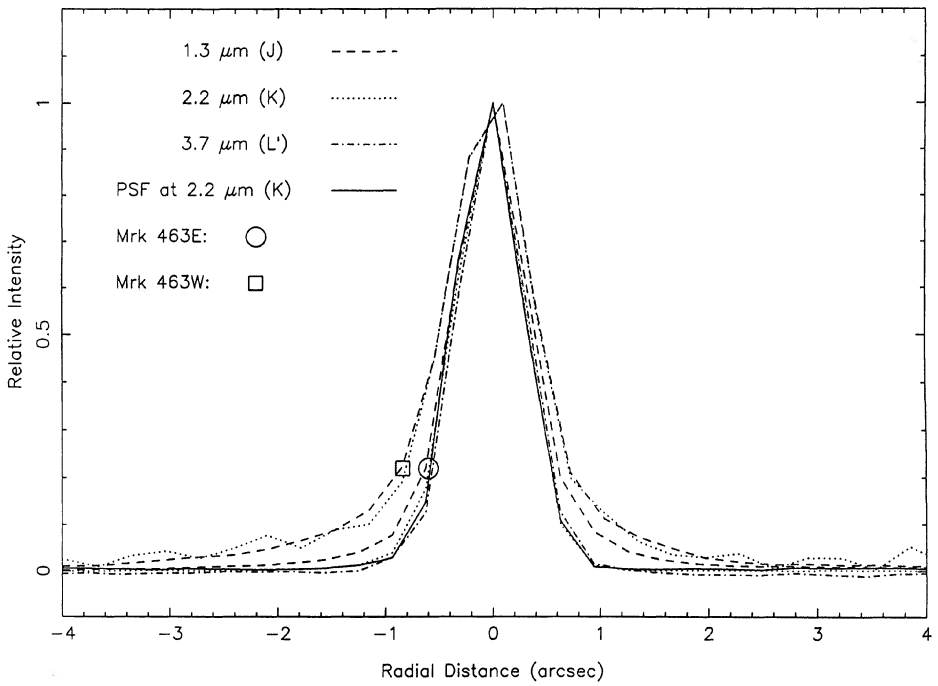

FIG. 10. Normalized brightness profiles of the nuclei compared to the point spread function (PSF). The emission profiles at *J*, *K*, and *L'* were normalized for each nucleus separately, and then the centers were shifted to compare with the PSF observed at *K*. The profiles were computed along the north–south direction to minimize overlap in the region between the nuclei. The solid line is the PSF at *K*, the dashed lines are the *J* band profiles, and the dotted lines are the *K* band profiles. The circle and square indicate the profiles of Mrk 463E and Mrk 463W, respectively.

Most observations suggest that Mrk 463W harbors an active nucleus as opposed to merely a starburst nucleus or extranuclear emission-line region. Optical spectra (Shuder & Osterbrock 1981; Hutchings & Neff 1989; Mazzarella & Boroson 1991) show that Mrk 463W has emission lines which are relatively broad (FWHM $\simeq$ 500 km s^{-1}). This line width is characteristic of Seyfert 2 nuclei, while most starburst nuclei have [O III] λ5007 line widths of FWHM $\lesssim$ 250 km s^{-1}. Diagnostic emission-lines (e.g., Veilleux & Osterbrock 1987) measured in total (unpolarized) optical flux reveal that Mrk 463W has line ratios of a Seyfert 2 nucleus. However, caution is due for two reasons. First, recent observations of Seyfert galaxies show that beamed or scattered ionizing radiation can produce an extranuclear high-ionization spectrum. In some cases the [O III]/Hα ratio is higher in extranuclear regions than in the Seyfert nuclei themselves (e.g., Wilson & Ulvestad 1982; Haniff *et al.* 1991). In the case of Mrk 463, the orientation of the radio/[O III] emission axis, and the optical polarization position angle of 82° observed by Miller & Goodrich (1990) provide strong evidence that a dust torus is aligned roughly along P.A. $\approx$ 80° in Mrk 463E. If the opening angle of the ionization cone is $\lesssim$ 30°, it is difficult to understand how Mrk 463E could be responsible for ionizing gas in the vicinity of Mrk 463W, which is 4 kpc away approximately normal to the radio axis. Additionally, Mrk 463W has a *K* band luminosity of $7.6\times10^9\ L_\odot$, characteristic of a luminous galaxy. The high-ionization, broad optical emission lines of Mrk 463W are therefore likely to be intrinsic to this independent nucleus. Second, although there is no doubt that Mrk 463W is a source of optical continuum and emission lines, spatial profiles of an optical long-slit spectrum suggests that bright, extended emission lines in Mrk 463E may contaminate the spectrum of Mrk 463W (Mazzarella & Boroson 1991). Therefore, the current optical data leave room for the possibility that Mrk 463W is a starburst nucleus.

The radio properties, unfortunately, do not provide an unambiguous discrimination between the AGN and starburst interpretations for Mrk 463W. The available radio data are best fitted with a power-law spectrum $f_\nu \propto \nu^{-0.5\pm0.1}$. It is common to find both Seyfert nuclei and starburst nuclei with such an index. The radio luminosity density of Mrk 463W is comparable with that of moderately luminous Seyfert galaxies (e.g., Ulvestad & Wilson 1984) and highly luminous starburst galaxies (e.g., Condon *et al.* 1991).

Some discrimination between the emission mechanisms in galactic nuclei is possible using their near-infrared colors, as illustrated in Fig. 11. While Mrk 463E is located in a region where only AGNs are found, the position of Mrk 463W leaves the nature of its dominant energy source ambiguous. Mrk 463W is redder in $H-K$ by 0.3 mag, but bluer in $J-H$ by 0.1 mag, than the mean of normal spiral galaxies. The circles in Fig. 11 represent galaxies in the *IRAS* Bright Galaxy Sample with $L_{\rm fir} > 10^{11}\ L_\odot$ (Carico *et al.* 1988, 1990a, 1990b) which are nearly all luminous starburst galaxies. Mrk 463W is $\approx$0.25 mag bluer in $J-H$ than the mean color for these galaxies. Weakly reddened free-free or power-law emission ($I_\nu \propto \nu^{-0.5}$) can explain such colors (e.g., Aaronson 1977). It is difficult to isolate which emission mechanism may be most important, but a power-law interpretation for the near-infrared colors is consistent with the other data that suggest Mrk 463W is a Seyfert nucleus.

4.4 The Role of the Galaxy Collision

The radio activity and high infrared luminosity have likely been triggered or enhanced by the galaxy collision taking place in Mrk 463. The extremely disturbed optical appearance, double nuclei, tidal tails, and the presence of three times the mass of the Milky Way in H_2 implies that Mrk 463 involves the close collision and likely ongoing merger of two gas-rich spiral galaxies. Recent *N*-body/hydrodynamical models of merging gas-rich galaxies suggest that gravitational torques may cause much of the gas to lose its angular momentum and collapse into the nuclear region (Barnes & Hernquist 1991). If this gas can lose substantially more angular momentum, perhaps by fragmentation and instabilities, a radial inflow rate sufficient to fuel an AGN may ensue (e.g., Shlosman *et al.* 1989). The simulations of Barnes & Hernquist also indicate that the formation of a stellar bar plays a substantial role in transporting angular momentum from the gas to the stars. It is interesting that the dominant morphological feature in the *J* band image of Mrk 463, other than the two nuclei, is a barlike formation [cf., Fig. 7(a)]. The direction of the winding of the tidal tails in Fig. 5 (see also Fig. 1, Hutchings & Neff 1989) suggests that both disks are rotating in a prograde orientation. This situation enhances the tidal distortions induced during galaxy mergers (Barnes & Hernquist 1991), providing further observational evidence that Mrk 463 manifests the properties predicted by models of the most violent galaxy collisions.

If the radio activity has been induced by the ongoing merger in Mrk 463, the age of the extended radio components must be less than or equal to dynamical age of the encounter. If the average jet velocity is $\sim10^4$ km s^{-1} (e.g., Wilson & Ulvestad 1982) and the axis is nearly in the plane of the sky, then the radio component 18 kpc to the south of Mrk 463E may be as young as $\sim2\times10^6$ yr. However, if deceleration due to ram pressure from the interstellar medium slowed the material to a few times 10^2 km s^{-1}, the source could have a minimum age as large as $\sim10^7$ yr. The models of Toomre & Toomre (1972) and Barnes & Hernquist (1991) indicate that tidal tails such as those observed in Mrk 463 are drawn out in the first $\sim10^8$ yr during an encounter between two similar mass disk galaxies. The interaction timescale is consistent with the hypothesis that the radio activity has been triggered by processes associated with the collision between the components of Mrk 463.

One puzzling problem with the ejection hypothesis for the radio structure in Mrk 463 is that the extended 20 cm emission to the northwest is not well aligned with the north–south axis of the other prominent radio features. Association of this emission with ejection from Mrk 463E would require a relatively complex model, perhaps invoking jet bending or interaction of collimated emission with the interstellar medium in Mrk 463W. An alternative possibility is that the northwest radio component and the emission apparently connecting it to the nuclear region are associated with ejection from Mrk 463W. Evidence was discussed above which suggests the western nucleus harbors a Seyfert nucleus which might be capable of producing the northwest radio source.

The evidence discussed here suggests that Mrk 463 represents a link between merging disk galaxies and quasars or radio galaxies. A nuclear starburst induced during the early stages of a merger might generate sufficient energy via radiation pressure, supernovae, or stellar winds to subsequently

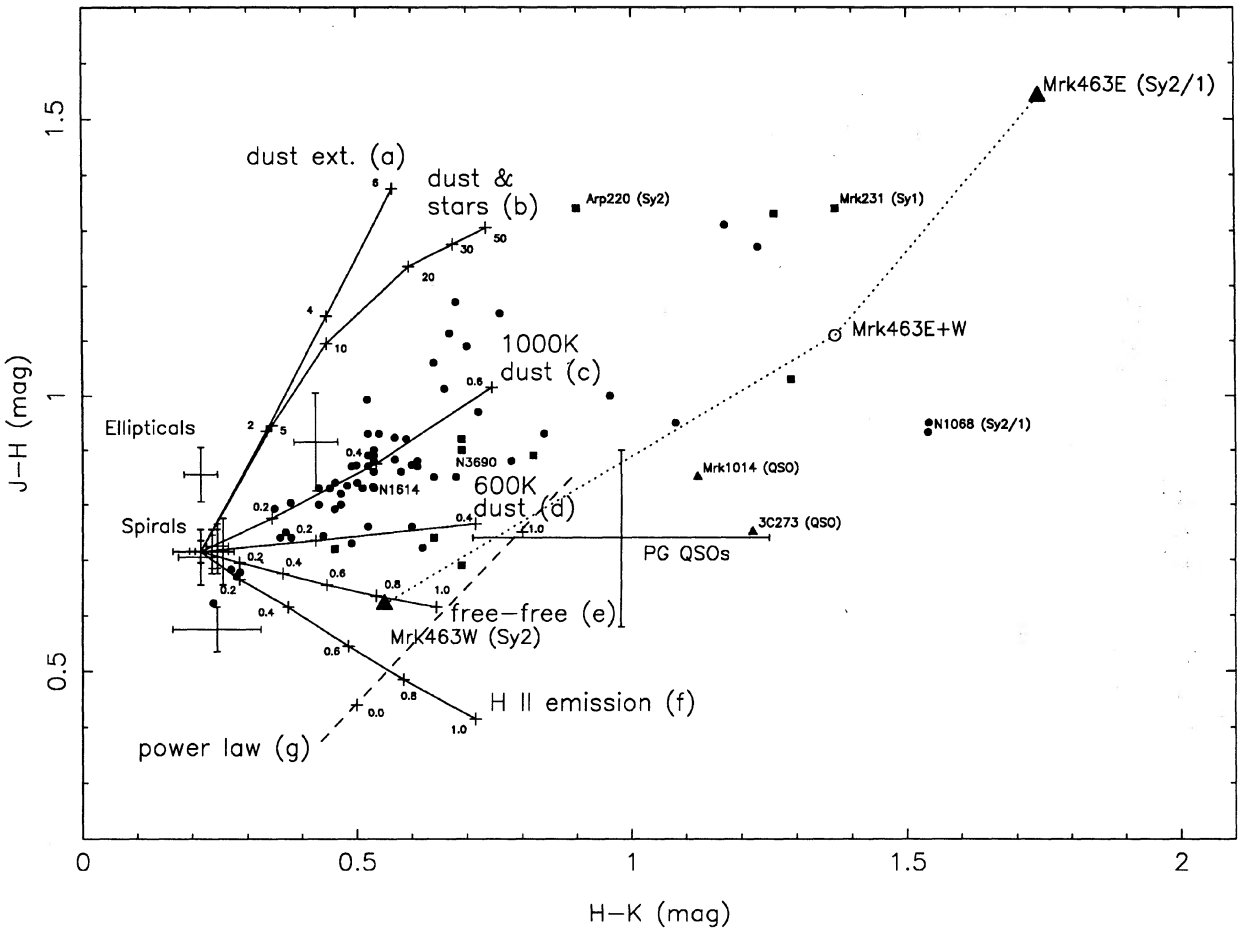

FIG. 11. Near-infrared color-color diagram showing the Mrk 463 integral system and nuclei (2″ beam measurements) in relation to normal and active galaxies. Mean values representative of normal spiral and elliptical galaxies and Palomar–Green quasars are indicated, where the error bars represent 1σ population dispersions of the distributions. The circles represent photometry (5″ diameter beam) for far-infrared luminous galaxies with $L_{\rm fir} > 10^{11}\,L_{\odot}$, and the squares are photometric data (2″5 and 5″ diameter beams) for the 10 ultraluminous galaxies of Sanders *et al.* (1988a). The data for the luminous and ultraluminous far-infrared galaxies are from Carico *et al.* (1988, 1990a, 1990b). The photometry for normal galaxies are from Aaronson (1977), and the data for PG quasars are from Neugebauer *et al.* (1987). Aaronson's photometry has been corrected to the CIT system for use here. The triangles indicate selected galaxies in the warm ultraluminous sample of Sanders *et al.* (1988b) with available photometry in Neugebauer *et al.* (1987). Optically determined nuclear activity types are from Sanders *et al.* (1988a; 1988b). Mrk 463E and NGC 1068 are labeled as "Sy2/1" to indicate their classification as Seyfert 1 nuclei based on their polarized optical spectra. Also plotted are models of various nonstellar effects from Fig. 24 of Aaronson (1977). The curves denote the following mechanisms: (a) reddening from a dust screen, labeled by the optical depth at V; (b) reddening due to dust mixed with stars, again labeled by the optical depth at V; (c) emission of dust with emissivity $\epsilon \propto \lambda^{-2}$ and a temperature of 1000 K, labeled by the fraction of contribution to K; (d) same as curve (c) except assuming 600 K dust; (e) free-free emission with an electron temperature of 20 000 K, labeled by the fractional contribution to K; (f) model of H II region emission with an electron temperature of 8000 K, again labeled by the fractional contribution to K; (g) pure power-law labeled by the spectral index n, where $I_{\nu} \propto \nu^{-n}$.

sweep out much of the dust and gas surrounding the nucleus (e.g., Sanders *et al.* 1988a, 1988b; Norman & Scoville 1988). This dispersing process might allow radio jets that would otherwise remain confined to the central few kpc to escape the nuclear region and form a classical extragalactic radio source with a large core-lobe distance. Observations and numerical simulations of advanced mergers such as NGC 7252 (Schweizer 1982; Borne & Richstone 1991) and Arp 220 (Wright *et al.* 1990) suggest they are in the process of relaxing into a single system which morphologically and kinematically looks like an elliptical galaxy. Mrk 463 and similar double-nucleus systems with small relative velocities appear to be earlier stages of ongoing mergers which, after $\sim 10^9$ yr, will experience a similar fate (e.g., Barnes & Hernquist 1991). If in certain cases luminous radio activity is triggered by the merger process, it is not a coincidence that powerful double-lobe radio galaxies are generally peculiar elliptical galaxies. If the interpretation of the extended radio sources as lobe-like structures is correct, then the ongoing merger taking place in Mrk 463 may represent the genesis of a classical radio galaxy or radio-loud quasar, consistent with previous indications of the important role of galaxy mergers in the formation of powerful radio galaxies (e.g., Baade & Minkowski 1954; Heckman *et al.* 1986).

5. SUMMARY AND CONCLUSIONS

5.1 Observational Results

(1) The two nuclei observed in optical images of Mrk 463 have been detected at 6 and 20 cm. The 20 cm luminosity density of the eastern nucleus, Mrk 463E, is 1.5×10^{24} W Hz^{-1}, which is characteristic of a quasar or radio galaxy. The radio luminosity of the western nucleus, Mrk 463W, is only $\approx1\%$ that of its companion; this is nevertheless comparable to a moderately luminous Seyfert galaxy or a highly luminous starburst galaxy. The radio flux densities of Mrk 463E and Mrk 463W are best fitted with power-law slopes α of -1.0 and -0.5 ($f_\nu \propto \nu^\alpha$), respectively. Mrk 463E is also a weak source of linearly polarized 20 cm emission, with 0.5% polarization at P.A. $\approx -45°$.

(2) A 20 cm image with 1".5 resolution and high dynamic range reveals components 4" north and 18" south of Mrk 463E. These sources are aligned with linear radio structure observed on scales of 0".05–1".5 (Neff & Ulvestad 1988), as well as extended conic [O III] emission (Hutchings & Neff 1989). A 20 cm source extending 10" to the northwest is also detected which is apparently linked to the nuclear region.

(3) Images at J, H, and K show the two galactic nuclei observed in the optical and radio images, but only Mrk 463E is detected at L'. The flux density of Mrk 463E dominates that of Mrk 463W with increasing wavelength. Mrk 463E has an L' luminosity of $\nu L_\nu(3.7\,\mu\text{m}) = 1.2\times10^{11}\,L_\odot$ and a $K-L'$ color of 2.1 mag, both of which compare to the median values for observed Palomar–Green quasars (Neugebauer *et al.* 1987). Mrk 463E has an extremely red $V-K$ color of 6.8 mag, which is nearly 3 mag larger than the reddest measured PG quasar.

(4) Near-infrared brightness profiles of Mrk 463E are unresolved at K and L' (radius $\lesssim0.4$ kpc), but extended at J, likely due to the effects of extinction and centrally concentrated hot dust emission ($T_d\sim800$ K). Resolved J and K brightness profiles associated with Mrk 463W indicate the near-infrared emission from this nucleus is predominantly due to extended starlight, with perhaps weak dust emission at $\lambda\gtrsim2.2\,\mu$m. Comparison of the $J-H$ and $H-K$ colors of Mrk 463W with normal disk galaxies and to far-infrared luminous galaxies reveals somewhat anomalous colors which may be modeled by a power-law source or free-free emission. Mrk 463E has extreme red $J-H$ and $H-K$ colors that are common only to AGNs.

5.2 Conclusions

The observation of radio continuum components 4 kpc north and 18 kpc south of Mrk 463E which are aligned with linear radio structure observed on scales of 0.05–1.5 kpc (Neff & Ulvestad 1988), as well as conic [O III] emission (Hutchings & Neff 1989), suggests that the central energy source in Mrk 463E is producing weak radio lobes. The 20 cm source to the northwest suggests that Mrk 463W may also be a source of collimated radio emission.

The spectral energy distribution and the 3.7 μm imaging data suggest that warm dust highly concentrated in the eastern nucleus dominates the far-infrared *IRAS* measurements for Mrk 463. A 20 cm luminosity density of 1.5×10^{22} W Hz^{-1}, compact 20 and 6 cm morphologies, and an $H-K$ color which is ≈0.3 mag redder than normal galaxies, are consistent with optical line ratios and line width measurements which indicate Mrk 463W is a Seyfert 2 nucleus. However, there is enough uncertainty in the current data that Mrk 463W may be a starburst nucleus. The projected size of the radio structure in Mrk 463 is an order of magnitude greater than seen in most Seyfert galaxies but comparable to low luminosity radio galaxies. The 20 cm luminosity and morphology suggest that Mrk 463 represents a transition between the confined radio sources in Seyfert nuclei and the widely extended radio structures observed in classical radio galaxies and quasars. Dilution of the interstellar medium in the host galaxy by supernovae, radiation pressure, or stellar winds triggered by a starburst may allow channeled radiation to escape greater distances than is possible in less active Seyfert galaxies which are not involved in violent mergers.

Centrally concentrated 2.2 and 3.7 μm dust emission, an extremely red $V-K$ color, and radio components aligned over the scale of 0.05–18 kpc, are all consistent with the presence of a dust torus which obscures an embedded quasar in Mrk 463E. The case for a hidden quasar is bolstered by a 3.7 μm luminosity and $K-L'$ color comparable to PG quasars, suggesting that the large $V-K$ color is largely due to visual extinction, and that Mrk 463E would appear as an optical quasar save for the obscuration. These data are consistent with the presence of an embedded Seyfert 1/quasar nucleus observed using optical spectropolarimetry (Miller & Goodrich 1990). In sum, these observations provide further support for a unified theory of AGNs in which the most luminous cases involve a causal connection between merging spiral galaxies, quasars, and radio galaxies.

We thank the night assistants at the Hale telescope, Juan Carrasco and Skip Staples, and the support staff of the Palomar Observatory and the VLA for assistance in obtaining the data. The imaging data were processed with AIPS and IRAF. We also thank James Ulvestad for an illuminating discussion about the sizes of radio structures in Seyfert galaxies, Charles Lawrence for helpful suggestions, and an anonymous referee for a number of useful comments. This research has made use of the NASA/IPAC Extragalactic Database (NED) which is operated by the Jet Propulsion Laboratory, California Institute of Technology, under contract with the National Aeronautics and Space Administration. This work was supported in part by a grant from the NSF, and by NASA through the Astrophysics Data Program and the Long Term Space Astrophysics Program.

REFERENCES

Aaronson, M. 1977, Ph.D. thesis, Harvard University
Adams, T. F. 1977, ApJS, 33, 19
Artyukh, V. S., and Vetukhnovskaya, Y. N. 1983, Pisma Astron. Zh, 9, 86
Baade, W., and Minkowski, R. 1954, ApJ, 119, 215
Barnes, J. A., and Hernquist, L. 1991, ApJL, 370, L65
Barthel, P. D. 1989, ApJ, 336, 606
Beichman, C., *et al.* 1985, ApJ, 293, 148
Borne, K. D., and Richstone, D. O. 1991, ApJ, 369, 111
Burstein, D., and Heiles, C. 1984, ApJS, 54, 33
Carico, D. P., Graham, J. R., Matthews, K., Wilson, T. D., Soifer, B. T.,

Neugebauer, G., and Sanders, D. B. 1990a, ApJL, 349, L39
Carico, D. P., Sanders, D. B., Soifer, B. T., Elias, J. H., Matthews, K., and Neugebauer, G. 1988, AJ, 95, 356
Carico, D. P., Sanders, D. B., Soifer, B. T., Matthews, K., and Neugebauer, G. 1990b, AJ, 100, 70
Condon, J. J. 1984, ApJ, 287, 461
Condon, J. J., Frayer, D. T., and Broderick, J. J. 1991, AJ, 101, 362
Cornwell, T., and Braun, R. 1989, in Synthesis Imaging in Radio Astronomy, edited by R. A. Perley, F. R. Schwab, and A. H. Bridle (Astronomical Society of the Pacific Conference Series, San Francisco), p. 167
Cornwell, T., and Fomalont, E. 1989, in Synthesis Imaging in Radio Astronomy, edited by R. A. Perley, F. R. Schwab, and A. H. Bridle (Astronomical Society of the Pacific Conference Series, San Francisco), p. 185
de Bryun, A. G., and Wilson, A. S. 1976, A&A, 53, 93
de Bryun, A. G., and Wilson, A. S. 1978, A&A, 64, 433
Elias, J. H., Frogel, J. A., Matthews, K., and Neugebauer, G. 1982, AJ, 87, 1029
Haniff, C. A., Ward, M. J., and Wilson, A. S. 1991, ApJ, 368, 167
Heckman, T. M., Smith, E. P., Baum, S. A., van Breugel, W. J. M., Miley, G. K., Illingworth, G. D., Bothun, G. D., and Balick, B. 1986, ApJ, 311, 526
Hill, G. J., Wynn-Williams, C. G., Becklin, E. E., and MacKenty, J. W. 1988, ApJ, 335, 93
Hutchings, J. B., and Neff, S. G. 1987, AJ, 93, 14
Hutchings, J. B., and Neff, S. G. 1989, AJ, 97, 1306
Hutchings, J. B., Gower, A. C., and Price, R. 1987, AJ, 93, 6
Kojoian, G., Sramek, R. A., Dickinson, D. F., Tovmassian, H., and Purton, C. R. 1976, ApJ, 203, 323
Mazzarella, J. M. 1989, Ph.D. thesis, University of Michigan
Mazzarella, J. M., and Boroson, T. A. 1987, BAAS, 19, 699
Mazzarella, J. M., and Boroson, T. A. 1991 (in preparation)
Miller, J. S., and Goodrich, R. W. 1990, ApJ, 355, 456
Neff, S. G., and Ulvestad, J. S. 1988, AJ, 96, 841
Neugebauer, G., Green, R. F., Matthews, K., Schmidt, M., Soifer, B. T., and Bennett, J. 1987, ApJS, 63, 615
Norman, C., and Scoville, N. 1988, ApJ, 332, 124
Peterson, B. M., Fricke, K., and Biermann, P. 1981, PASP, 93, 28L
Petrosian, A. R., Saakian, K. A., and Khachikian, E. E. 1978, Afz, 14, 69
Phinney, E. S. 1989, in Theory of Accretion Disks, edited by P. Meyer, W. Duschl, J. Frank, and E. Meyer-Hofmeister (Kluwer, Dordrecht), p. 451
Sanders, D. B., Soifer, B. T., Elias, J. H., Madore, B. F., Matthews, K., Neugebauer, G., and Scoville, N. Z. 1988a, ApJ, 325, 74
Sanders, D. B., Soifer, B. T., Elias, J. H., Neugebauer, G., and Matthews, K. 1988b, ApJL, 328, L35
Sanders, D. B., Scoville, N. Z., Zensus, A., Soifer, B. T., Wilson, T. L., Zylka, R., and Steppe, H. 1989, A&AL, 231, L5
Schweizer, F. 1982, ApJ, 252, 455
Shlosman, I., Frank, J., and Begelman, M. C. 1989, Nat, 338, 45
Shuder, J. M., and Osterbrock, D. E. 1981, ApJ, 250, 55
Toomre, A., and Toomre, J. 1972, ApJ, 178, 623
Ulvestad, J. S. 1990, private communication
Ulvestad, J. S., and Wilson, A. S. 1984, ApJ, 285, 439
Ulvestad, J. S., and Wilson, A. S. 1989, ApJ, 343, 659
Ulvestad, J. S., Wilson, A. S., and Sramek, R. A. 1981, ApJ, 247, 419
Unger, S. W., Pedlar, A., Booler, R. V., and Harrison, B. A., 1986, MNRAS, 219, 387
Veilleux, S., and Osterbrock, D. E. 1987, ApJS, 63, 295
Wilson, A. S., and Ulvestad, J. S. 1982, ApJ, 260, 56
Wilson, A. S., and Willis, A. G. 1980, ApJ, 240, 429
Wright, G. S., James, P. A., Joseph, R. D., and McLean, I. S. 1990, Nat, 344, 417